remote sensing

MDPI

Article

Unmanned Aerial Systems (UAS)-Based Methods for Solar Induced Chlorophyll Fluorescence (SIF) Retrieval with Non-Imaging Spectrometers: State of the Art

Juan Quirós Vargas [1,*], Juliane Bendig [2], Alasdair Mac Arthur [3,4], Andreas Burkart [5], Tommaso Julitta [5], Kadmiel Maseyk [6], Rick Thomas [7,8], Bastian Siegmann [1], Micol Rossini [9], Marco Celesti [9], Dirk Schüttemeyer [10], Thorsten Kraska [11], Onno Muller [1] and Uwe Rascher [1]

1 Institute of Biogeosciences, IBG2: Plant Sciences, Forschungszentrum Jülich GmbH, 52425 Jülich, Germany; b.siegmann@fz-juelich.de (B.S.); o.muller@fz-juelich.de (O.M.); u.rascher@fz-juelich.de (U.R.)
2 School of Technology, Environments and Design, University of Tasmania, Hobart, TAS 7001, Australia; juliane.bendig@utas.edu.au
3 School of Geosciences, University of Edinburgh, Edinburgh EH9 3FF, UK; Alasdair.MacArthur@ed.ac.uk or alasdair.macarthur@uv.es
4 Laboratory for Earth Observation, Image Processing Laboratory, University of Valencia, 46980 Valencia, Spain
5 JB Hyperspectral Devices UG, Am Botanischen Garten 33, Düsseldorf 40225, Germany; andreas@jb-hyperspectral.com (A.B.); tommaso@jb-hyperspectral.com (T.J.)
6 School of Environment, Earth & Ecosystem Sciences, The Open University, Milton Keynes MK7 6AA, UK; kadmiel.maseyk@open.ac.uk
7 Birmingham Institute of Forest Research (BIFoR), University of Birmingham, Birmingham B15 2TT, UK; rick@bigskyscience.com
8 Big Sky Science Ltd., Sutton Coldfield B72 1SY, UK
9 Remote Sensing of Environmental Dynamics Laboratory, Department of Earth and Environmental Sciences (DISAT), University of Milano-Bicocca, Piazza della Scienza1, 20126 Milano, Italy; micol.rossini@unimib.it (M.R.); marco.celesti@unimib.it (M.C.)
10 ESA-ESTEC, 2201 AZ Noordwijk, The Netherlands; dirk.schuettemeyer@esa.int
11 Field Lab Campus Klein-Altendorf, University of Bonn, 53359 Rheinbach, Germany; kraska@uni-bonn.de
* Correspondence: j.quiros@fz-juelich.de

Received: 14 April 2020; Accepted: 13 May 2020; Published: 19 May 2020

Abstract: Chlorophyll fluorescence (ChlF) information offers a deep insight into the plant physiological status by reason of the close relationship it has with the photosynthetic activity. The unmanned aerial systems (UAS)-based assessment of solar induced ChlF (SIF) using non-imaging spectrometers and radiance-based retrieval methods, has the potential to provide spatio-temporal photosynthetic performance information at field scale. The objective of this manuscript is to report the main advances in the development of UAS-based methods for SIF retrieval with non-imaging spectrometers through the latest scientific contributions, some of which are being developed within the frame of the Training on Remote Sensing for Ecosystem Modelling (TRuStEE) program. Investigations from the Universities of Edinburgh (School of Geosciences) and Tasmania (School of Technology, Environments and Design) are first presented, both sharing the principle of the spectroradiometer optical path bifurcation throughout, the so called 'Piccolo-Doppio' and 'AirSIF' systems, respectively. Furthermore, JB Hyperspectral Devices' ongoing investigations towards the closest possible characterization of the atmospheric interference suffered by orbital platforms are outlined. The latest approach focuses on the observation of one single ground point across a multiple-kilometer atmosphere vertical column using the high altitude UAS named as AirFloX, mounted on a specifically designed and manufactured fixed wing platform: 'FloXPlane'. We present technical details and preliminary results obtained

from each instrument, a summary of their main characteristics, and finally the remaining challenges and open research questions are addressed. On the basis of the presented findings, the consensus is that SIF can be retrieved from low altitude spectroscopy. However, the UAS-based methods for SIF retrieval still present uncertainties associated with the current sensor characteristics and the spatio-temporal mismatching between aerial and ground measurements, which complicate robust validations. Complementary studies regarding the standardization of calibration methods and the characterization of spectroradiometers and data processing workflows are also required. Moreover, other open research questions such as those related to the implementation of atmospheric correction, bidirectional reflectance distribution function (BRDF) correction, and accurate surface elevation models remain to be addressed.

Keywords: hyperspectral remote sensing; light weight spectroradiometer; telluric bands; ESA-FLEX; VNIR; SIF; UAS

1. Introduction

Chlorophyll fluorescence (ChlF) is defined as the light emitted by photosynthetic organisms with peaks at 687 (red ChlF) and 740 nm (far-red ChlF) [1]. The study of ChlF goes further than the estimation of basic structural plant traits like those usually analyzed from conventional multispectral remote sensing [2], e.g., throughout vegetation indices based on red-green-blue (RGB) and near infrared (NIR) reflectance. ChlF occurs in competition with heat to dissipate absorbed radiation not used in the light reactions of photosynthesis. Thus, the variation in the efficiency of one process affects the efficiencies of the others. This link forms the rationale for the use of ChlF to infer the plant physiological status, improving the understanding of the health ↔ stress status dynamics of plants in agricultural and environmental studies [3]. Recent studies successfully used ChlF as a proxy for water stress [4], leaf nitrogen [5], nutrient status [6], biomass determination [7], and gross primary production (GPP) [8]. The authors of [9] summarize the main physiological processes, such those related to photo-protection, that might be affected by specific ChlF drivers at ecological and temporal scales.

Several options are available for the assessment of ChlF, such as the light induced fluorescence transient (LIFT) active sensing method, which provides accurate ChlF field estimations especially useful in the context of high-throughput phenotyping field experiments [10]. However, this proximal technique is not viable for open field studies, as it is only suitable for close range observations. Large scale monitoring becomes feasible with the passive sensing of solar induced ChlF (SIF) [9] on the basis of hyperspectral techniques using spectroradiometers, e.g., on airborne and orbital platforms [11]. SIF can be quantitatively obtained throughout spectral measurements by the Oxygen-A (O_2-A, 760 nm) and Oxygen-B (O_2-B, 687 nm) absorption features of the atmosphere, where the ratio between the ChlF signal and the reflected radiance is higher [12] due to the absorption of the incoming irradiance (>90% in O_2-A) [2,9]. SIF is considered the most direct remote sensing signal to infer the actual functional state of the photosynthetic apparatus and its dynamics at leaf, canopy, ecosystem, or even global scale. However, the SIF–photosynthesis relationship is influenced by several factors, including environmental conditions, structural traits, stress effects, and re-absorption processes by chlorophyll [9]. Hence, ancillary information is needed to interpret fluorescence changes and link them to variations in the photosynthetic efficiency. Moreover, an accurate retrieval of SIF is crucial to understand photosynthesis and its dynamics [13]. The three main SIF retrieval methods are: the Fraunhofer Lines Depth (FLD) [14], the spectral fitting methods (SFM) [15], and the singular vector decomposition (SVD) [16].

The relatively low intensity of the ChlF signal (<1%–5% of the reflected NIR radiation) [2] makes the retrieval of SIF challenging, and numerous studies tried to address this. Satellite missions, for example the Orbiting Carbon Observatory-2 (OCO-2), the Gases Observing Satellite (GOSAT), and the Global Ozone Monitoring Experiment-2 (GOME-2) were used to retrieve SIF for the assessment

of physiological parameters like carbon fixation [17,18]. Other missions such as the Scanning Imaging Absorption Spectrometer for Atmospheric Cartography (SCIMACHY), the Tropospheric Monitoring Instrument (TROPOMI), and the Exploratory Satellite for Atmospheric CO_2 (TanSat) have been used for similar purposes [19]. Airborne SIF estimations are also being explored by means of the HyPlant sensor: a system composed by two spectroradiometers covering the 400–2500 nm and 670–780 nm spectral ranges [20]. During the last years, HyPlant data has been the subject of a number of preliminary studies [21–23] related to the FLuorescence EXplorer (FLEX) mission of the European Space Agency (ESA) [24]. The first validated HyPlant maps were published in 2015, where contrasting SIF values among crops were found and attributed to differences in the photosynthetic apparatus activity [25]. Further studies reported the relation between HyPlant-derived SIF information and GPP [26]. Moreover, Tagliabue et al. [8] recently generated GPP maps over a forest area based on SIF retrieved from HyPlant imagery. They found significant correlations among SIF, GPP and absorbed photosynthetically active radiation in a range of $R^2 = 0.43$–0.46 ($p < 0.001$).

The interpretation and validation of space-borne and airborne SIF retrievals rely on the comparison with field measurements [27]. Yet, there is a scaling difference between these levels of observation that could possibly be addressed by unmanned aerial systems (UAS) [28] due to their intermediate sensor-surface distance. In a wide review of the existing remote sensing studies to retrieve top-of-canopy SIF, the authors of [29] commented about the lack of literature about UAS-based developments, and the lack of systematic protocols for data processing leading to uncertainties. Zarco-Tejada et al. [30] simulated the effect of aggregated reflectance on satellite imagery by decreasing the pixel size of low altitude hyperspectral data. These authors found that the correlation between key physiological traits, specifically stomatal conductance and ChlF, was reduced from $R^2 = 0.69$ ($p < 0.01$) to $R^2 = 0.38$ ($p < 0.05$) when using the original UAS imagery and the decreased spatial resolution image, respectively. In a similar approach, in the study of [31] they flew up to 500 m above ground level (AGL) to simulate satellite-like conditions for SIF retrieval, but only preliminary results were presented without a deeper insight in the high altitude results.

Contrary to UAS based imaging sensors, the technical feasibility for field measurements of non-imaging spectrometers [32], combined with their higher signal to noise ratio (SNR) and higher spectral and dynamic resolutions (allowing quantitative ChlF retrievals), as well as the reduced size and energy consumption encouraged employing these systems on UAS for SIF retrieval [33]. This concept has been in development for the past eight years, and notably in the last three to five years, it has been materialized in UAS models and prototypes leading to encouraging results. Nevertheless, further investigations are necessary until the point of a full operational UAS for SIF retrieval is reached. Thus, the aim of the present manuscript is to communicate the state of the art and future challenges in the development of UAS-based methods for SIF.

The manuscript is organized in four sections. Section 2 presents an overview of previous efforts using UAS-mounted spectroradiometers for reflectance measurements. In Section 3, the main three projects for UAS-based retrieval of SIF are presented: 'Piccolo Doppio' [34,35], 'AirSIF' [36], and 'FloXPlane' [37]. Section 4 is dedicated to a discussion about remaining challenges and open research questions.

2. Previous Efforts with UAS-Mounted Spectroradiometers for Reflectance Measurements

Ground based spectroradiometer measurements can be carried out relatively easily following standard protocols for setup, calibration, and data storage. When the instrument is mounted on an aerial platform, the accurate footprint (defined as the sampled Earth surface area from which radiance is received) geolocation on the ground, and the measurement of ambient light changes during the flight become the main challenges, which have been addressed in previous studies from different perspectives:

(a) Burkart et al. [38] calculated reflectance based on synchronized measurements from two, one on-board and one on-ground, equally configured and cross calibrated STS micro-spectroradiometers (STS Series Spectrometers, Ocean Optics, Dunedin, Florida, USA) under the same environmental conditions. In this case, the radiometric calibration was performed indirectly from comparisons

between STS and an Analytical Spectral Device (ASD) FieldSpec 4 (Analytical Spectral Devices, Inc., Boulder, Colorado, USA) calibrated spectroradiometer. Results proved the high precision of the reasonably priced STS measurements, notwithstanding a second order effect was detected influencing NIR readings. The 338–412 nm stray light interfered with bands within 676–823 nm, especially in the O_2-A band. Consequently, the authors suggested additional studies for STS-based SIF retrieval. Current investigations are focused on the use of STS micro-spectroradiometers, not for SIF measurements, but for the assessment of reflectance factors as a complementary (canopy scale) data source to leaf level spectral information acquired with an ASD spectroradiometer. The system, from the Environmental Remote Sensing and Spectroscopy Laboratory (SpecLab), included a real time optimization of the integration time, seeking to maximize signal independently of target brightness or changes in illumination. This feature was relevant considering the low signal-to-noise ratio of the STS spectrometers, and the variability of surface reflectance factors in heterogeneous Mediterranean tree-grass ecosystems, where bright dry grass is mixed with dark tree canopies during summer [39].

(b) Garzonio et al. [40] realized downwelling irradiance measurements with a USB4000 spectroradiometer (Ocean Optics, Dunedin, Florida, USA) through linear interpolation of two measurements of the radiance reflected by a reference tarp, and the use of a second on-ground hand held ASD FieldSpec measuring a Lambertian surface (Spectralon®) as reference (both spectroradiometers were synchronized). The robust radiometric and spectral calibration of the instruments, despite not being temperature stabilized (e.g., the STS and the USB4000), permitted accurate radiance measurements especially at O_2-A. Both approaches present a relative root mean square error lower than 10% compared with ground information.

3. Currently Operational UAS Systems for SIF Retrieval

3.1. "Piccolo-Doppio"—A Dual-Field of View (FOV) Dual Spectrometer System

Remote sensing protocols for accurate SIF retrieval, based on high spectral resolution data at the oxygen absorption features, require the sunlight irradiance (downwelling) and surface energy emissions (upwelling) being simultaneously measured. These measurements generally mismatch in time in a range of multiple seconds, thus causing uncertainties in the SIF estimation. To overcome this, Mac Arthur et al. [34] split the fore optic path into a QEPro spectroradiometer (Ocean Optics, Dunedin, Florida, USA) aiming at a dual FOV system as proposed by [41]. The sensor measures in the 650–800 nm spectral range at a resolution of 0.15 nm, with a full width at half maximum (FWHM) between 0.31 and 0.35 nm. The SNR, dynamic range, and integration times are: 1000:1, 8.5×10^4:1, and up to 60 min, respectively. The detector has 1048×64 pixels (two-dimensional) with columns summed to give increased dynamic range (Table 1). The system, named Piccolo-Doppio, is capable to perform upwelling and downwelling (cosine error <2%) measurements almost simultaneously (≈50 ms difference between each measurement), diminishing reported uncertainties in field readings [42]. Moreover, the capability to work with two spectroradiometers (with a double bifurcated fiber optic assembly) differentiates the Piccolo-Doppio from some other UAS-based methods, since it allows synchronized Visible and NIR (VNIR; 400–950 nm) and the SIF (640–800 nm) measurements using the same fore optic for upwelling and the same fore optic for downwelling readings. Thus, any VNIR index, e.g., the photochemical reflectance index (PRI), can be derived together with SIF. As a drawback, light transmittance is reduced in one channel (either upwelling or downwelling) as fibers of two different diameters have been used which increases integration times and reduces SNR of the channel with the smaller diameter fiber. The use of one spectrometer, rather than two with independent optical paths, is necessary (i) to avoid the interpolation of one wavelength scale to the other (which might lead to loose detail in particular across the O_2 absorption features); and (ii) to ensure the radiometric calibration is constant for both up and downwelling measurements.

Table 1. Summary of the main characteristics of the spectroradiometer and UAS utilized for each project.

Platform		Spectroradiometer		Additional Components	Unmanned Aerial System (UAS)		Highlights
Piccolo-Doppio	QEPro (Ocean Optics, Inc., USA)	Dimensions	182 × 110 × 47 mm	Radio control for data transferring	Custom hexacopter	Tarot T910 frame KDE 4213 motors pixhawk autopilot	Can be used with two spectroradiometers
		Spectral range (nm)	650–800	Battery Lithium Polymer 14.7 V, 1 A			Two independent channels
		Approximate spectral interval (nm)	0.15	Originally a raspberry Pi Model A. Currently updated to Pi3	Custom quadcopter	T-motor U8 100 kv motors Pixhawk autopilot Based on a Gryphon dynamics frame	Dual FOV for NIR reflectance and SIF (O_2-A/O_2-B)
		FWHM (nm)	0.31 (5 μm optical slit)–0.35 (10 μm optical slit)	RTK or PPK correction	DJI Matrice 600 A3 Pro	Dimensions: 1.67 × 1.52 × 0.75 m	Upwelling and downwelling measurements near simultaneously
		Digital range (analogue to digital converter; bit)	18			Payload 6 kg (16 min hovering)	Etaloning effect correction.
		SNR	1000:1			take-off weight 15 kg	Feasible installation on aerial and ground based platforms
		Dynamic range	8.5×10^4:1			Vertical and horizontal hovering accuracy 0.5 m and 1.5 m	
		Integration time	up to 60 min			Vertical take-off and landing	DJI GNS- RTK system (3 GPS antenna)
	Has been tested with:	NIRQuest, QEPro, Flame, HR4000 and Maya				3 GNSS antennas and IMU's	
AirSIF	QEPro (Ocean Optics, Inc., USA)	Dimensions	182 × 110 × 47 mm	Dual GNSS antenna	DJI Matrice 600	Dimensions: 1.67 × 1.52 0.75 m	Adaption of the two independent channels system
		Spectral range (nm)	500–870	IMU		Payload 7 kg	Characterization of cosine corrector homogeneity and linearity
		Approximate spectral interval (nm)	0.37	Grasshopper 3 machine vision camera		take-off weight 15 kg	Upwelling and downwelling measurements near simultaneously
		FWHM (nm)	0.80	RTK correction		Vertical and horizontal hovering accuracy 0.5 m and 1.5 m	NIR reflectance and SIF (O_2-A/O_2-B)
		Digital range (bit)	18			Average flight speed: 2 m/s	Etaloning effect correction
		SNR	1000:1			Vertical take-off and landing	Dual GNSS antennae for accurate georeferencing in post processing
		Dynamic range	8.5×10^4:1				

Table 1. *Cont.*

Platform		Spectroradiometer		Additional Components	Unmanned Aerial System (UAS)		Highlights
AirFloX/ FloxPlane	QEPro (Ocean Optics, Inc., USA)	Dimensions	182 × 110 × 47 mm	Data acquisition module	FloXPlane: large fixed wing	Wingspan 4.40 m	The QEPro is integrated with a large but light UAS capable to elevate several kilometers with one spectrometer coupled
		Spectral range (nm)	650–800			Length 3.32 m	
		Approximate spectral interval (nm)	0.17	Independent battery management		take-off weight 24 kg	
		FWHM (nm)	0.30	Stabilizing gimbal		Payload 2.5 kg	
		Digital range (bit)		GPS times stamps for synchronizing		Battery weight 9 kg	
		SNR	1000:1			Average cruise speed: 10 m/s	Single spot constant monitoring
		Dynamic range	8.5×10^4:1			- Endurance: 1.5 h normal cruise flight. High altitude 40 min.	Characterize SIF retrieved at very high altitude for a closer understanding of satellite-based estimations
						Runway length of about 10 m for start and landing.	

Figure 1 summarizes the main steps to process Piccolo-Doppio data, from the extraction of JavaScript Object Notation (JSON) files into MATLAB® (Mathworks, Field Spectroscopy Facility Post Processing Toolbox) [43] to the multiplication of the radiance (or irradiance) by the non-linearity corrected, the normalized, and the dark current corrected values per pixel for each spectroradiometer and optical direction. Currently, the data processing workflow and codes are updated to Python3.

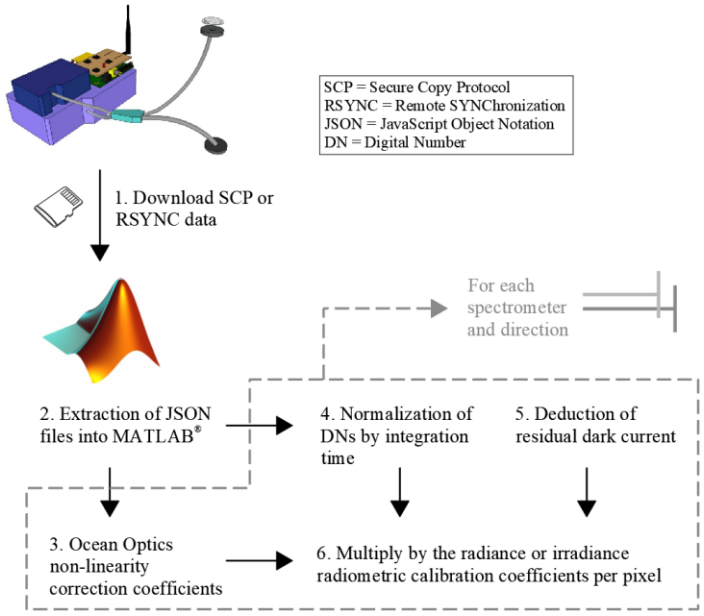

Figure 1. Piccolo-Doppio data processing workflow to obtain radiance. In step 2, an analogue data processing flow was developed in Python3.

Alongside the software solutions, the authors worked on hardware developments, e.g., the design of the fore optic and fiber optic assembly in order to maximize the light transmission, thus achieving integration times of 50–75 ms at VNIR, and 500–1500 ms at SIF wavelengths under clear-sky conditions in northern Europe (when the spectroradiometer's maximum dynamic range is utilized). Nonetheless, the QEPro is prone to the etaloning effect caused by the interference of the light reflected in the boundaries of its thinned back-illuminated charge coupled device [42] detector, consequently producing wavy-aspect outputs. Founded on the statements of the instrument's near-linear response to light intensity (when the generic non-linearity correction of the instrument is applied to the data in post processing) plus the etaloning stationarity in respect to the wavelength, [34] carried out laboratory experiments and presented two post-processing techniques for the etaloning correction for any system using QEPro spectrometers:

(i) 'By reference': employing etaloning correction factors obtained from the division between the measured spectra of a calibrated light source and the known outputs per wavelength. The factors were applied to tungsten halogen readings at 20 levels of intensity (Figure 2a). The instrument response was then convolved with the respective spectral measurements to obtain the spectrum with the etaloning effect corrected. A variance of ±0.7% was detected (Figure 2b) and linked to the instrument non-perfect linear response.

(ii) 'By curve-fitting and residual interpolation': using correction coefficients obtained from the rounded residuals between actual and spline-smoothed reflectance at 17 levels of intensity of a tungsten halogen light source. A validation test performed with three additional levels of intensity demonstrated the efficiency of the method by reproducing a smooth spectrum (Figure 2c). Furthermore, the residuals of measured wavelengths were interpolated to enable the etaloning correction at unassessed ranges. The results obtained, differed by no more than 10 raw digital

counts (DN) from the etaloning corrected spectra (Figure 2d), hence demonstrating higher performance in the correction of the effect compared with the 'referencing' method.

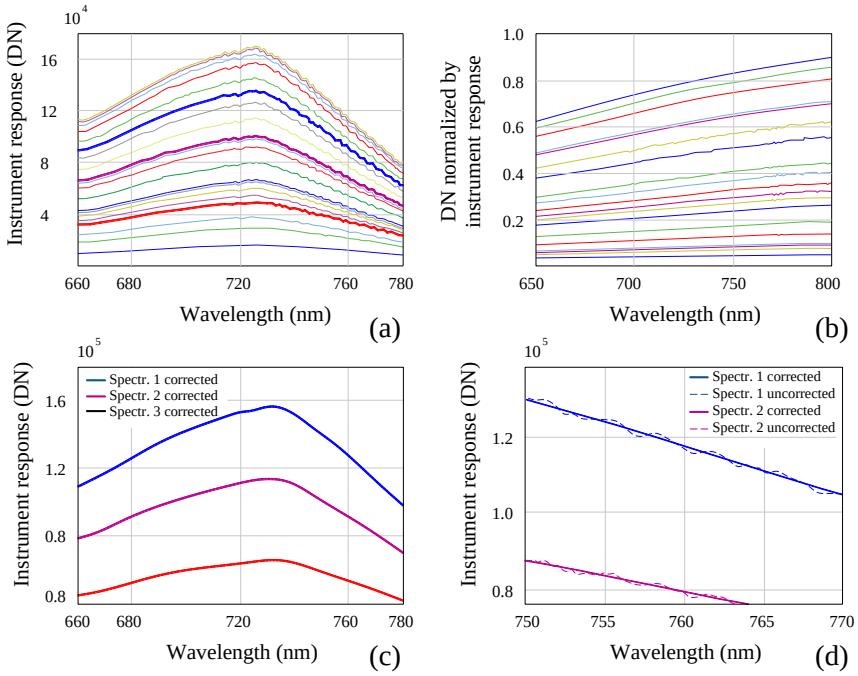

Figure 2. (**a**) Uncorrected spectral measurements of 20 light intensity levels of the tungsten halogen calibrated light and (**b**) their respective 'by-reference' corrected wavelengths. (**c**) Presents the 'by curve-fitting and residual interpolation' corrected spectra of the three curves highlighted in (**a**) with the same colors, and the detailed example of corrected vs. uncorrected instrument response is shown in (**d**) [34].

Mac Arthur et al. [34] demonstrated a feasible route to solve the discrepancies in time between surface radiance and solar irradiance wavelengths collected from individual spectroradiometers. The authors clarified that the application of both methods for etaloning correction under field conditions is challenging and will necessitate to push the spectroradiometer dynamic range to the maximum. Later, the authors of [33] reported the feasibility to mount the Piccolo-Doppio onto the UAS DJI Matrice 600 with an interchangeable gimbal where the spectroradiometer could be installed together with an RGB or thermal camera (Figure 3a). The Piccolo-Doppio design was further used by [31] who recorded information at several altitudes (up to 500 m) and time points confirming the viability of the Piccolo-Doppio system to be mounted on aerial platforms. However, at the time of the present manuscript publication the authors had not completed the data processing.

Additionally, a Piccolo-Doppio was also installed on a DJI Matrice 600 Pro [44] to monitor SIF in a mature oak woodland (UK) over a 30 m diameter free air CO_2 enrichment experiment [45]. A significant correlation of $R^2 = 0.8821$ ($p < 0.01$; Figure 3b) was found between UAS-based SIF and the incoming radiation, suggesting reliable variations of the SIF data retrieved with this system especially in a context where other approaches (e.g., eddy covariance) are not appropriate due to the scale of the treatments. Additionally, SIF information was useful to identify treatment effects and its relationship with environmental drivers.

Furthermore, the spectral calibration and characterization of three spectroradiometers using a Piccolo-Doppio-like system design could be analyzed [46] by the implementation of two methodologies, using Ar and Ne lamps or a double monochromator respectively. The versatility of Piccolo-Doppio makes it practical to be used even on a ground platform mounted on a tractor, as demonstrated by [47] who estimated soy bean populations on early vegetative states under changing atmospheric conditions.

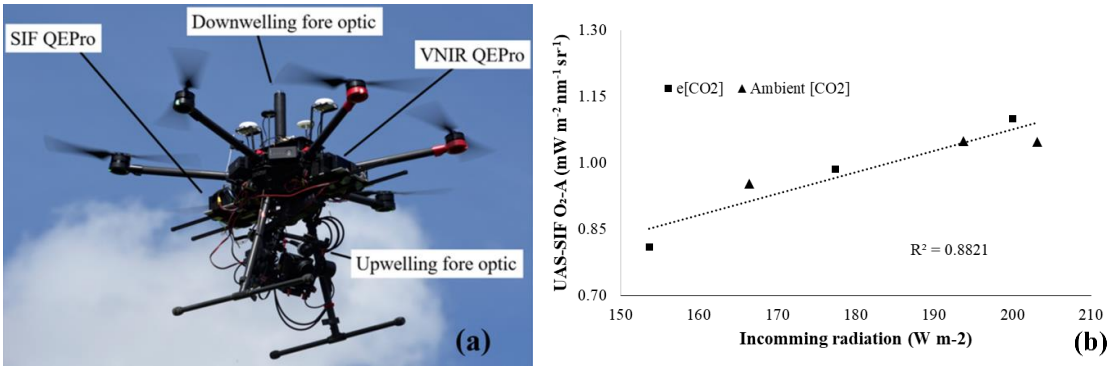

Figure 3. (**a**) Instrument presented by [33] and used by [31,44], highlighting the position of the solar induced ChlF (SIF) QEPro, downwelling and upwelling fore optics and VNIR QEPro (source: Dr. Andrew Revill, BBSRC/NERC ATEC project at University of Edinburgh-GeoSciences); and (**b**) the relationship between incoming radiation and SIF under ambient and elevated [CO_2] in a mature oak forest, measured at the BIFoR FACE site in the UK.

3.2. "AirSIF"—A UAS-Based Spectroradiometer

The AirSIF platform (Figure 4a) shares the Piccolo-Doppio concept of splitting the optical path but using a single spectroradiometer (500–870 nm spectral range at an interval of 0.37 nm, with a FWHM of 0.8 nm), for collecting real time downwelling and upwelling radiance. AirSIF includes a dual global navigation satellite system (GNSS) antenna. Furthermore, in [36] the authors implemented the etaloning effect correction suggested by [34]. Additionally, they retrieved the corrected zenith angle between sun and cosine corrector (Ocean Optics CC-3), and the fore optic measuring downwelling radiance, depending on sun position and inclination of the cosine corrector during the UAS flight [28]. This information was computed from the platform pitch, roll and yaw obtained from an inertial measurement unit (IMU) mounted next to the cosine corrector. Cosine corrector measurements were not influenced by the azimuth angle, but sun zenith angles of >10° resulted in a significant deviation from the expected cosine response of the cosine corrector. Common flight conditions led to platform tilt angles of 6° maximum. In order to correct the uncertainty caused by the irradiance underestimation of the cosine corrector, the authors of [28] proposed to estimate a corrected zenith angle based on the dot product principle accounting for the two vectors involved: the vectors between cosine sensor and sun and the cosine corrector pointing direction. With the implementation of this function mean and maximum differences of 1.7% and 3.2% from the original radiance measurements were obtained.

The latest results presented in March 2019 by [48] at the International Network on Remote Sensing of Terrestrial and Aquatic Fluorescence conference, reported the results of a comparison between AirSIF-derived spectra measured at 8 m AGL over barley experiment plots versus ground-based SIF retrieved with a high-resolution references system, the Fluorescence Box (Flox, JB Hyperspectral Devices, Düsseldorf, Germany) [37] mounted on a field-bike (Figure 4b). The results are visualized in a map of spatially explicit and geolocated AirSIF footprints with their respective O_2-A SIF ranges at edge and middle sampled plots overlaid over an orthophoto derived from UAS imagery (Figure 4c). Flox footprints were estimated as round shapes, where the size was estimated from sensor height above canopy according the 25° FOV of the Flox instrument. The study had four main shortcomings: (i) the spatial misalignment of the footprints between repeated UAS flights, (ii) the lack of accurate geolocation of Flox ground measurements, (iii) the difference in footprint size between AirSIF and Flox (0.5–2.5 m^2), and (iv) the resulting significant difference between UAS- and Flox-based SIF measurements. The accuracy of the footprint determination of the AirSIF platform was analyzed in a recent study being ±15 cm for 10 m AGL height [49].

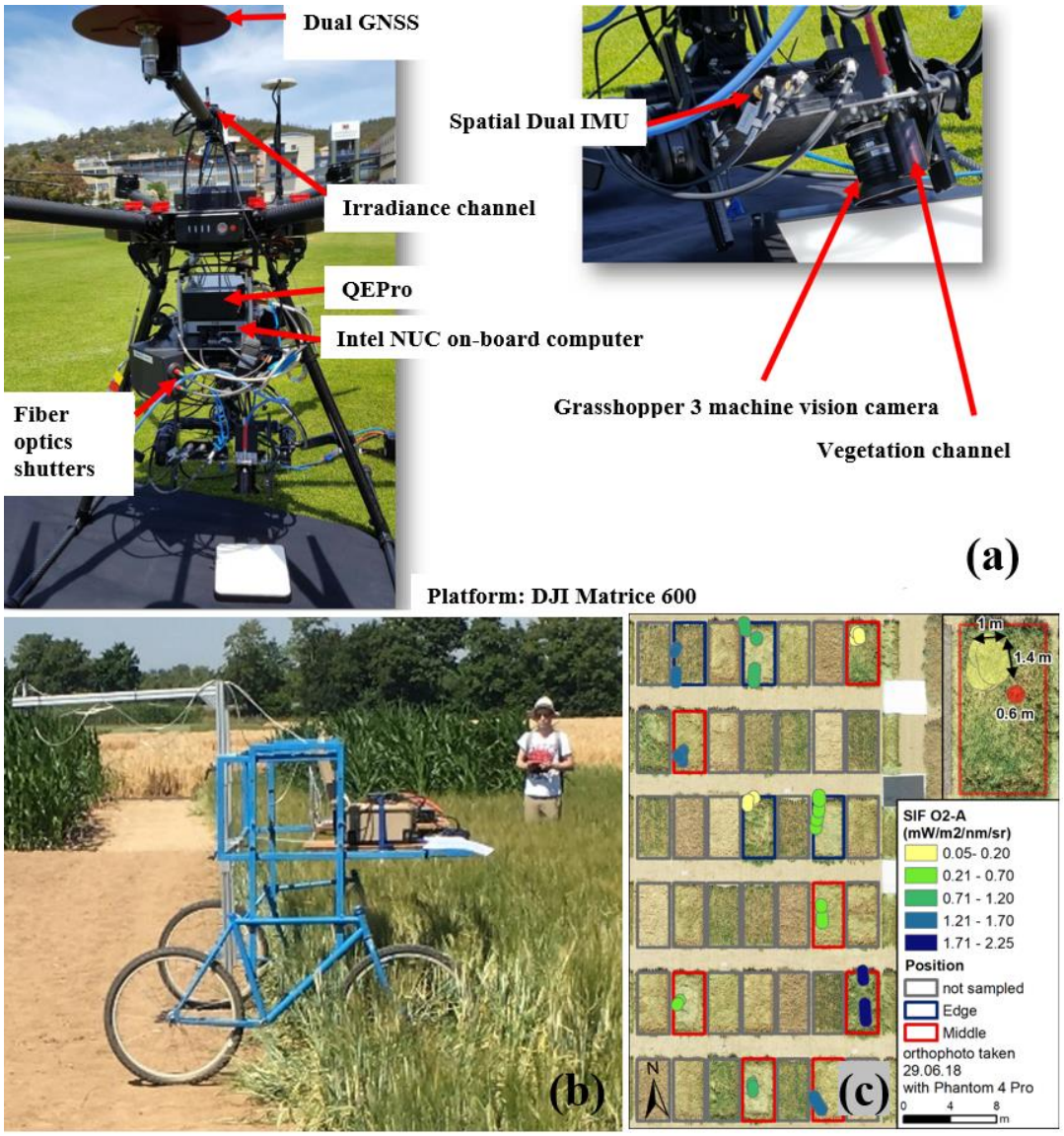

Figure 4. (**a**) AirSIF system components, (**b**) field bike used for ground Flox measurements, and (**c**) footprints of the flight at 12:00 local time with their respective O_2-A SIF at edge (blue) and middle (red) sampled plots over the orthophoto derived from UAS photogrammetry [49].

An initial test was carried out by comparing a single AirSIF flight with Flox observations from the field bike. The measurements were collected at the Campus Klein-Altendorf, an agricultural research station affiliated to the Agricultural Faculty of the University of Bonn (Germany). In total, 55 observations over nine 3 × 5 m barley plots were collected, three per plot by the Flox instrument, and between one and four per plot by AirSIF at 10:45–12:00 (Flox) and 12:00–12:15 (AirSIF), respectively. The results showed a link between the SIF retrieved from both platforms, which was stronger but negative for UAS footprints located at the plot edge (Figure 5a). A paired *t*-test showed no significant differences between the mean SIF retrieved from UAS and Flox. Moreover, there seems to be an underestimation of ≈13% with UAS-based measurements (Figure 5b).

The implementation of a dual GNSS antenna system [50], the use of an IMU in the correct position, and the appropriate flight and sensor configurations [51] were found crucial to acquire the highest accuracy in the platform pose characterization and footprint localization for the improvement of SIF estimates, especially over small experimental plots like the ones presented here. Consequently,

the authors of [52] published the results of research concerning boresight (IMU-spectroradiometer-camera misalignment) and lever arm (GNSS antenna-spectroradiometer offset) correction methods.

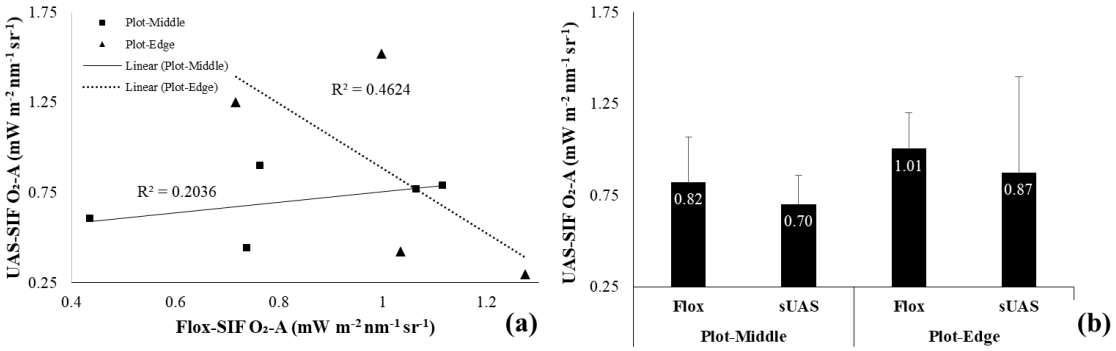

Figure 5. (**a**) Linear regression and (**b**) comparison between mean values of Flox instrument and UAS SIF measurements. Flox footprints were always located at the center of the plots, and UAS footprints were at the middle and edge of the plots.

3.3. "AirFloX" on Board of the "FloXPlane"—Atmospheric Interference on SIF Retrieval Across a Multiple Kilometer Air Column

The AirFloX is the lighter and simplified version of the Flox system manufactured by JB Hypersectral Devices [53], and up to date the only existing commercially available instrument for the continuous long-term top of canopy SIF measurements. Whilst FloX design, reported in [54], relies on the use of two channels to collect nearly simultaneously upwelling and downwelling at sensor radiance, AirFloX is designed to only acquire data collected by one channel (downward looking fiber), making it more similar, in a conceptual approach, to an image sensor. Due to the distance from the canopy at which the sensor is expected to fly, up to 4 km, the upwelling at sensor radiance is expected to be biased by atmospheric absorption, thus not easily used for SIF retrieval. The fluorescence retrieval will be performed by applying a similar processing scheme as the one used in imaging sensors data processing, e.g., HyPlant [20].

The investigations described here, alongside airborne (HyPlant) studies for SIF retrieval, contribute to integrate into the bigger picture of the FLEX satellite mission expected to be launched in 2022 [55]. Within this context, one of the major challenges is to precisely understand the impact of large atmosphere columns on a kilometer scale and their impact on SIF retrieval. Background studies started elucidating this topic, as presented by [56], who showed that SIF is strongly influenced by the atmospheric scattering and absorption, which in turn are defined by factors such as the surface pressure and concentration of aerosols. In practice, the higher the sensor-surface distance, the larger the air column above the targets [19], the stronger the scattering and the extinction of the signal in the atmosphere due to the absorption by aerosols and oxygen molecules, respectively. Hence, at this multiple km vertical scale, retrieving SIF becomes more challenging due to the need of increasing the accuracy of the atmospheric correction.

Recently, researchers from JB Hyperspectral Devices developed a high altitude and light fixed wing UAS, called 'FloXPlane' (Figure 6a), equipped with the AirFloX system (Figure 6b,c). The FloXPlane was manufactured with two purposes: (i) sampling large areas suitable for satellite calibration/validation (cal/val), and (ii) characterizing the surface radiance of one fixed spot at ground level across a multiple kilometer (up to 4000 m) air column. Their goal is to measure the atmospheric absorption of the upwelling SIF emission, considering that the majority of oxygen and aerosols are present in the innermost atmosphere layers. This is achieved by a steep screw-like flight pattern, incorporating a stabilizing gimbal, which ensures accurate pointing of the sensor to the target. A co-aligned camera provides proof of the gimbal pointing accuracy and allows structure from motion processing for highly accurate positioning of the sensor in 3D space. Using a fixed wing aircraft turned out to be mandatory

for this mission, since it can provide enough range to reach 4 km and will sail down to ground level. This concept ensures the necessary safety and fallback scenarios to achieve legal clearance into public airspace.

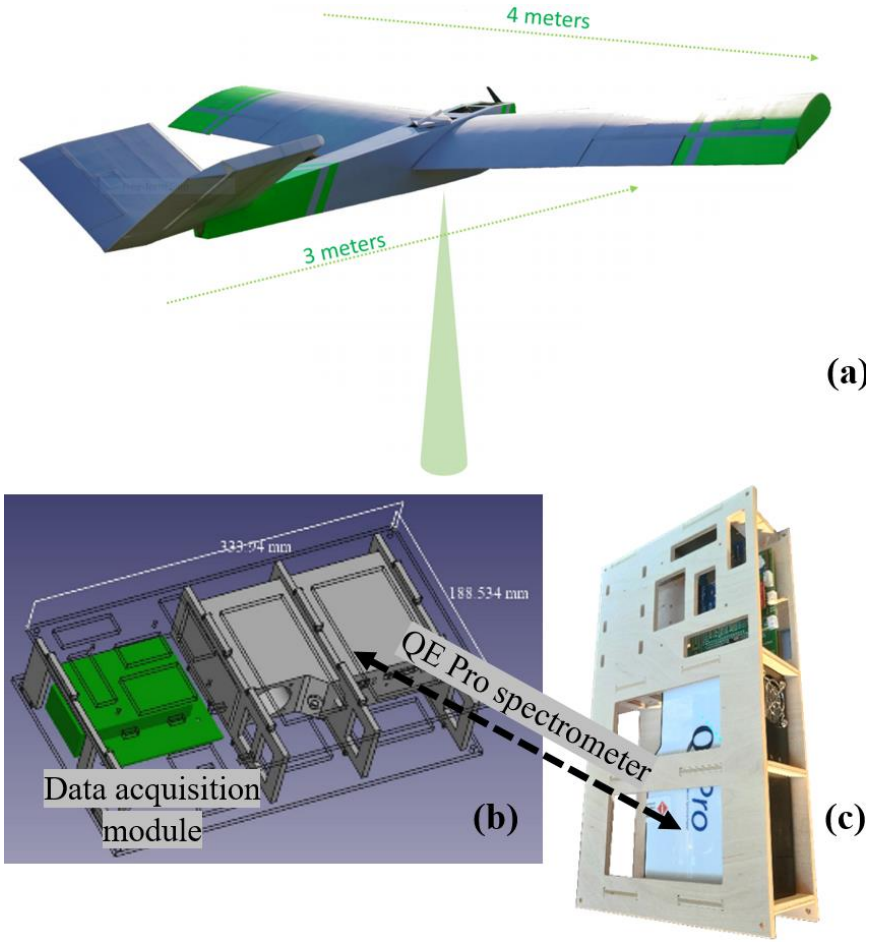

Figure 6. The FloXPlane fixed wing UAS (**a**), equipped with AirFloX system (**b**,**c**).

At the time of writing, the complex legislation process allowing the experimental UAS flights in the controlled airspace has been successful. However, in this manuscript the results of previous tests flying to a maximum altitude of 600 m AGL are shown. Further experiments with the AirFloX system onboard a manned aircraft, a manned gas balloon, and a rotary wing DJI Matrice 600 have been performed in 2018 and 2019. A focus of the medium-altitude vertical flights is the determination of the change in the O_2-A and O_2-B absorption versus the distance from the target (i.e., flight altitude). In fact, the change of absorption in these two bands is directly affecting the SIF estimates, therefore, an accurate parametrization is a key factor for accurate SIF retrieval using flying platforms. Due to the changing light conditions during flights, the absolute oxygen band depth value could lead to erroneous results. Therefore, the relative band depth was calculated as reported in the following formula:

$$Band\ depth = \frac{L\lambda out - L\lambda in}{L\lambda out} \quad (1)$$

where $L\lambda out$ and $L\lambda in$ are the wavelength of the shoulder and the deepest point of the oxygen absorption band, respectively. Preliminary results reported in Figure 7 are promising. The O_2-B and O_2-A at sensor radiance spectra (Figure 7a,b) show a stable spectral and radiometric behavior i.e., no spectral shift caused by grating distortion due to air pressure is found.

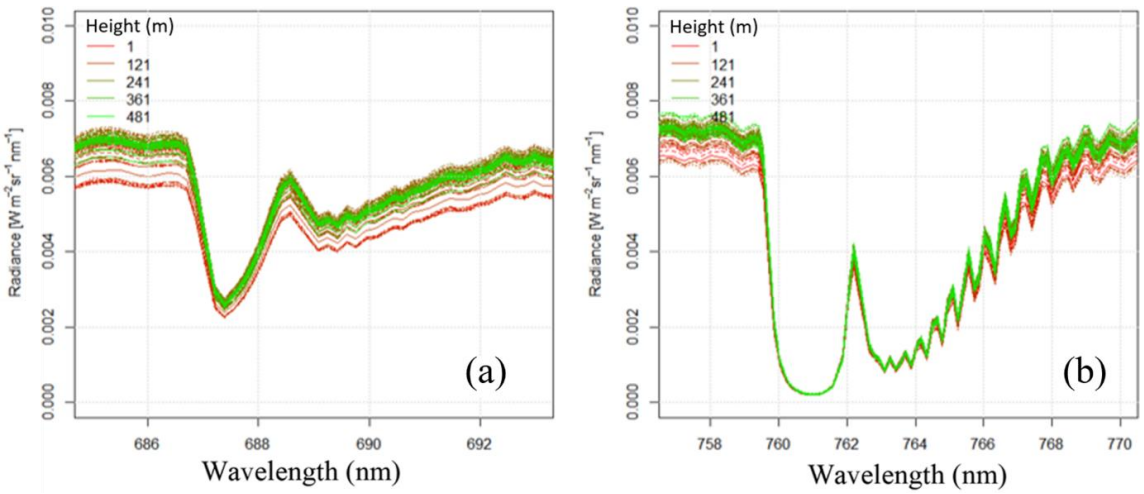

Figure 7. Zoom to the (**a**) O_2-B and (**b**) O_2-A at sensor radiance spectra of the first flight of the FloX-Plane UAS [36].

As shown in Figure 8, the two flights performed were made on a 600 m vertical column. A pseudo normalized difference vegetation index (NDVI; at sensor radiance based) was calculated showing that the target was remaining the same during the whole ascending flight duration (bare soil). The invariant target selection is a key point, since no confounding SIF emission is expected to alter the oxygen band depth. Looking at the relative band depth change, an increase of 1% was found in the O_2-B band, whilst for O_2-A results are less clear. Although the preliminary results are aligned with theory, a stronger absorption takes place under a larger air column leading to SIF underestimations [57]. Thus, the encouraging results obtained hitherto support the needs of more and repeated flights, covering a wider range of atmospheric conditions (e.g., different solar zenith angle ranges, aerosol concentrations, and air pressure conditions).

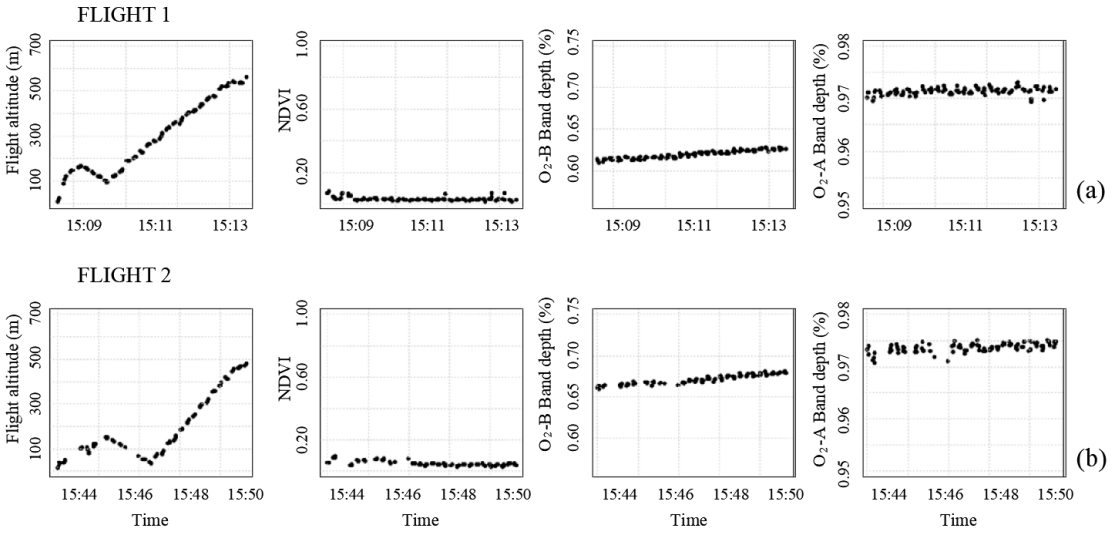

Figure 8. Flight altitude, pseudo-NDVI, and O_2-A and O_2-B relative bands depth for the (**a**) first and (**b**) second preliminary flights up to 600 m AGL. The first plots on each panel show the relation between the time and the flight altitude.

3.4. Summary of the UAS-Based Methods Presented

The presented projects are summarized in Figure 9, where the main components of the Piccolo-Doppio, AirSIF, and FloXPlane are displayed. The figure tracks the progress in development

of UAS-based platforms for quantitative retrieval of SIF in physical units starting with the fiber optic bifurcation of [34], who also conducted a valuable characterization of the etaloning effect, and afterwards adapted by [35,36] who installed a similar-principle system on-board a UAS including the implementation of an IMU and a dual GNSS antenna for a better pose characterization and cosine corrector performance analysis. Researchers from [37] added the investigation of the atmospheric influence on SIF retrieval under a 600 m air column.

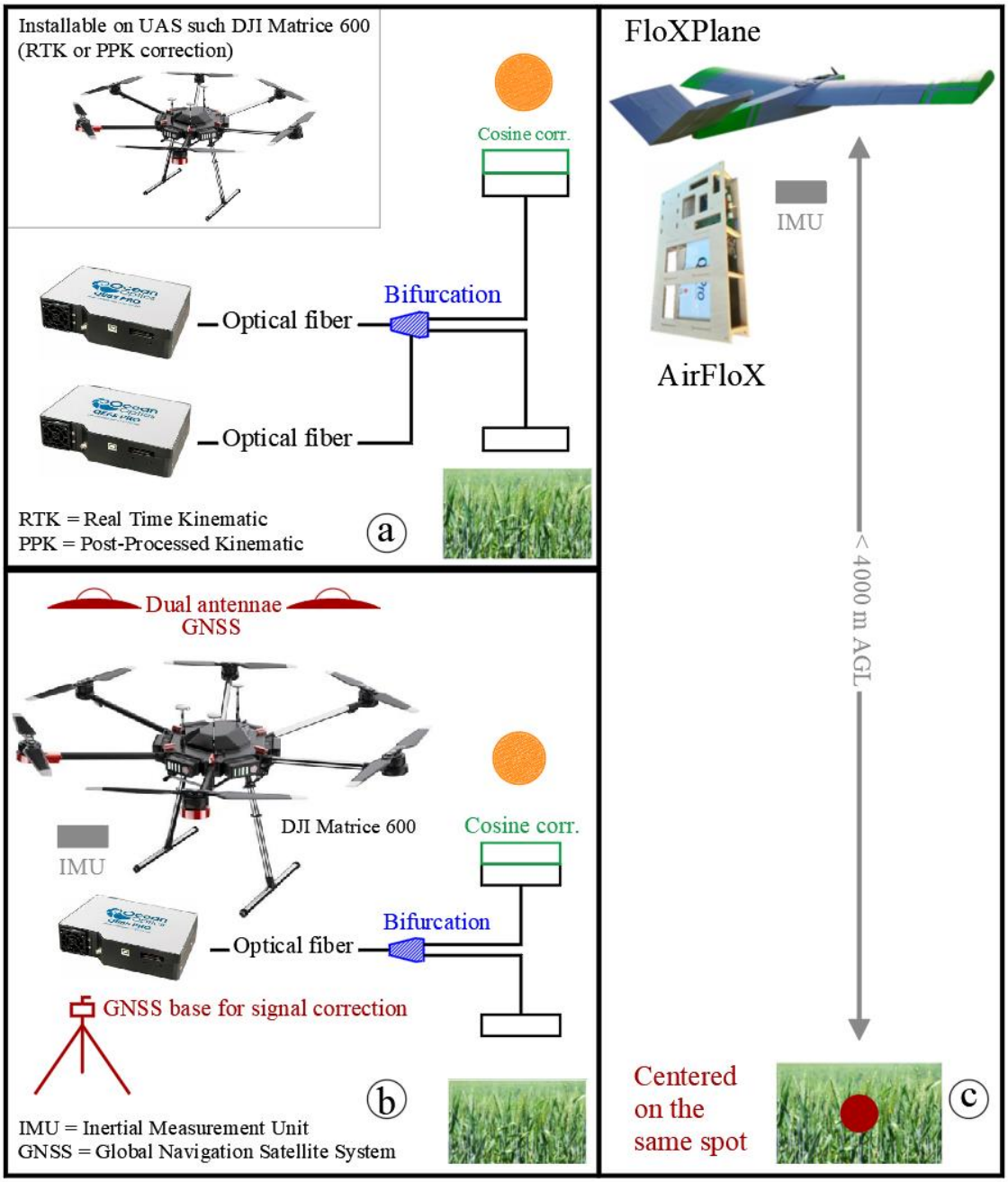

Figure 9. Schemes summarizing the main characteristics of (**a**) Piccolo-Doppio, (**b**) AirSIF, and (**c**) FloXPlane.

More systems may be under development, e.g., a platform called FluorSpec, not discussed here, is currently being developed by researchers of the Geo-information Science and Remote Sensing laboratory, at Wageningen Unversity and Research [58]. The core components of the system are the QEPro spectrometer, an RGB camera, a GNSS, and a Laser rangefinder sensor, all boarded on a DJI

S1000 octocopter. The spectrometer is configured with a split fiber, one channel for downwelling and one for upwelling measurements, covering a spectral range from 630 to 800 nm, with an FWHM of 0.14 nm and a spectral sampling interval of 0.31 nm. The irradiance, radiance, and reflectance factors at the top of UAS and canopy level can be derived after radiometric calibration and atmospheric correction processing.

4. Remaining Challenges and Open Research Questions

Beyond the valuable advances achieved so far, several challenges are yet to be overcome and several issues related to the UAS-based methods for SIF retrieval remain open. First, the sensitivity of the cosine corrector to varying sun zenith angles, and the etaloning effect caused by the interfering of the light reflected in the borders of the back-illuminated thinned charge coupled device add uncertainty to SIF estimations. In addition, sensor calibration methods, data collection, and data processing protocols need to be standardized and spectroradiometers need to be characterized [46] in order to enable measurements from different instruments at diverse geographical locations and temporal periods to be directly compared. The main features to be characterized are the FWHM as proposed by [42], and the SNR, spectral sampling interval, and spectral shift, which were identified by [59] as the most impacting characteristics on SIF retrieved with FLD methods. Besides, inherent issues of the SIF retrieval must be considered, such as the higher variation and lower SNR generally obtained in the O_2-B, and the lack of required information to run an accurate correction to diminish the effect of atmospheric interference.

Besides the sensor-associated issues, complementary studies should be conducted suggesting ways to improve the FOV geolocation accuracy, and the spatio-temporal match between on-board and proximal measurements of same targets. Indeed, robust validations of UAS-based SIF estimations are up to now hindered by these spatio-temporal discrepancies of the two levels of information, since their comparison is not fully convincing with differences of few meters and/or minutes. Some ideas have been proposed to improve the spatio-temporal match between UAS-based and ground SIF retrievals aiming at conclusive validations; for instance, in [40] the authors suggest to overlay the spectrometer data with RGB imagery derived maps, while the authors of [51] recommend the use of real time kinematic (RTK) correction for the geolocation of footprints, plus the implementation of lever arm and boresight corrections [52].

Moreover, the precise characterization of the spectroradiometer footprint might also be achieved with the support of automated ground platforms for SIF assessment, particularly those developed and used in plant phenotyping. These instruments can be programmed to collect SIF data at specific points with an accuracy of few seconds and centimeters, which consequently can be precisely aligned with the moment and place of the UAS-based data points. Some ground platforms for SIF phenotyping can be configured to collect information at specific sensor angles and AGL elevation, therefore they might also be used for optimal UAS flight simulations with a precise pose characterization and footprint spatio-temporal location, targeting to (i) elucidate the real maximum scope of UAS-based methods for SIF retrieval, which is so far unclear, (ii) facilitate the robust validation of aerial retrievals, thus (iii) allowing deeper analyses and understanding of the SIF estimated from low altitude hyperspectral data, e.g., throughout the comparison of retrieval methods, and a thorough comprehension of the sensor multi-angularity effect.

Furthermore, according to [60], the effect of the atmospheric conditions should be incorporated into the retrieval throughout model-based approaches notwithstanding if the data is acquired at proximal, airborne, or orbital level, which opens another query: would the accuracy of UAS-based SIF retrievals be significantly increased by implementing new dedicated atmospheric correction methods where current models are not easily adapted? In addition, the authors of [61] reported the impact of the bidirectional reflectance distribution function (BRDF) on the canopy chlorophyll content estimation from UAS hyperspectral imagery. The authors recommend the correction of the BRDF for reliable and consistent estimations, as it accounts for the surface reflectance anisotropy and varying solar and instrument-view angles. Although the authors of [61] used an imaging sensor, the same principle

applies to the UAS-mounted point spectrometers [62] since the BRDF effect is inherent to remote sensing information [63].

Pinto et al. [63] studied the SIF directionality according to the surface, inclination, and orientation of leaves, as well as the sensor and sun angles. Nonetheless, the authors worked with single and static measurements, therefore a full characterization of the BRDF was not possible due to the limited range of illumination and viewing angles. In this respect, hypothetically, the implementation of a detailed canopy slopes map computed from a UAS-derived crop surface model might contribute to upscale and improve the results found by [63]. Moreover, considering that surface elevation differences of 0.50–1.50 m AGL (common crop canopy height range) represent 5%–15% of the sensor-surface distance in low altitude (e.g., 10 m AGL) UAS flights, we can also hypothesize that the incorporation of a crop surface model into the UAS-based methods for SIF assessment might help to better account for the ChlF re-absorption effect. Accordingly, more scientific questions arise: does the implementation of accurate surface elevation models significantly improve the quality of SIF estimations? Could a slope map derived from a crop surface model represent the canopy architecture complexity? Might this be useful for a full canopy BRDF characterization thus precise SIF retrievals from UAS-based methods?

5. Conclusions

The UAS-based retrieval of SIF with non-imaging spectroradiometers is possible and has been demonstrated by a number of groups. Recent advances in the platform and instrument design contributed:

(i) The optical path bifurcation presented in the Piccolo-Doppio system for nearly simultaneous upwelling and downwelling measurements with two spectroradiometers, allowing synchronized VNIR and SIF measurements.

(ii) The implementation of a dual GNSS antenna system and IMU placed in the correct position, alongside the appropriate flight and sensor configurations reported in the AirSIF project, for the accurate pose characterization and footprint geolocation accuracies.

(iii) The development of the FloXPlane as a fixed wing UAS for very high altitude measurements, which will provide crucial information to understand the impact of large atmosphere columns on the retrieval of SIF.

Despite many important advances achieved by [34,36,37], UAS-based SIF observations from non-imaging spectroradiometers still present uncertainties associated to the current sensor characteristics and the spatio-temporal mismatching between aerial and ground measurements, mostly caused by the footprint spatial extent and form and location dependency on the flying height and pose geometry. The latest complicated the proper robust validation of aerial UAS-SIF measurements. Consequently, more investigations are required addressing the accurate FOV size and location, along with the spatio-temporal matching of UAS-based and ground SIF measurements of the same targets. Complementary studies regarding the standardization of calibration methods and the characterization of spectroradiometers and data processing workflows are required. Open research questions like those related to the implementation of atmospheric correction, BRDF correction, and accurate surface elevation models should be addressed in the future.

Author Contributions: Conceptualization, J.Q.V., U.R., M.R., M.C.; investigation, J.B., A.M.A., A.B., K.M., R.T.; writing—original draft preparation, J.Q.V.; writing—review and editing, J.Q.V., J.B., A.M.A., T.J., B.S., M.R., M.C., T.K.; supervision, U.R., O.M., B.S., M.R., M.C.; project administration, M.R., M.C., D.S., T.K.; funding acquisition, M.R., M.C, U.R., O.M., D.S. All authors have read and agreed to the published version of the manuscript.

Funding: The research has received funding from the European Union's Horizon 2020 research and innovation program under the Marie Sklodowska-Curie grant agreement no. 721995. This document was prepared within the Training on Remote Sensing for Ecosystem Modelling (TRuStEE) consortium. The "AirFloX" on board of the "FloXPlane" system (Section 3.3) is founded by the European Space Agency (ESA) project number 4000120771: Technical Assistance for the Development of Ground-based Systems for Long term measurements of Red and Far-red Sun Induced chlorophyll Fluorescence (DEFLOX).

Acknowledgments: The authors acknowledge the contribution of Kai Wittneben as collaborator in the development of the FloXPlane at JB Hyperspectral Devices; Zbyněk Malenovský, Deepak Gautam, and Arko Lucieer at the

University of Tasmania for the development of AirSIF; Magnus Hagdorn and Richard Taylor at University of Edinburgh, Scotland, Iain Robinson at RAL, UK and Luis Alonso at University of Valencia, Spain, for their contribution to the Piccolo-Doppio project. We thank to Maria Pilar Martin, Na Wang, and Lammert Kooistra, the first from the Environmental Remote Sensing and Spectroscopy Laboratory (SpecLab), Spanish National Research Council (CSIC), and the latest two from the Geo-information Science and Remote Sensing laboratory, at Wageningen University and Research (WUR), for their support sharing information about the SpecLab and FluorSpec ongoing investigations, respectively. We also acknowledge the contribution of the Field Lab Campus Klein-Altendorf (CKA), University of Bonn, for their support enabling field experiments for the data collection of the AirSIF study case.

Conflicts of Interest: The authors declare no conflict of interest.

Abbreviations

The following abbreviations are used in this manuscript:

AGL	Above ground level
ASD	Analytical spectral device
BRDF	Bidirectional reflectance distribution function
ChlF	Chlorophyll fluorescence
DN	Raw digital counts
ESA	European Space Agency
FLD	Fraunhofer Lines Depth
FLEX	FLuorescence EXplorer
Flox	Fluorescence box
FOV	Field of view
FWHM	Full Width at Half Maximum
GNSS	Global navigation satellite system
GOME-2	Global Ozone Monitoring Experiment–2
GOSAT	Gases Observing Satellite
GPP	Gross primary production
IMU	Inertial measurement unit
JSON	JavaScript Object Notation
LIFT	Light induced fluorescence
NDVI	Normalized difference vegetation index
NIR	Near infrared
O_2-A	Oxygen-A band
O_2-B	Oxygen-B band
OCO-2	Orbiting Carbon Observatory-2
PRI	Photochemical reflectance index
RGB	red-green-blue
SCIMACHY	Scanning Imaging Absorption Spectrometer for Atmospheric Cartography
SFM	Spectral fitting method
SIF	Solar induced chlorophyll fluorescence
SNR	Signal to noise ratio
SpecLab	Environmental Remote Sensing and Spectroscopy Laboratory
SVD	Singular vector decomposition
TanSat	Tropospheric Monitoring Instrument (TROPOMI) and the Exploratory Satellite for Atmospheric CO_2
TRuStEE	Training on Remote Sensing for Ecosystem Modelling
UAS	Unmanned aerial systems
VNIR	Visible and near-infrared

References

1. Kalaji, H.M.; Schansker, G.; Brestic, M.; Bussotti, F.; Calatayud, A.; Ferroni, L.; Goltsev, V.; Guidi, L.; Jajoo, A.; Li, P.; et al. Frequently asked questions about chlorophyll fluorescence, the sequel. *Photosynth. Res.* **2017**, *132*, 13–66. [CrossRef] [PubMed]

2. Meroni, M.; Rossini, M.; Guanter, L.; Alonso, L.; Rascher, U.; Colombo, R.; Moreno, J. Remote sensing of solar-induced chlorophyll fluorescence: Review of methods and applications. *Remote Sens. Environ.* **2009**, *113*, 2037–2051. [CrossRef]
3. Murchie, E.; Kefauver, S.; Araus-Ortega, J.L.; Muller, O.; Rascher, U.; Flood, P.; Lawson, T. Measuring the dynamic photosynthome. *Ann. Bot.* **2018**, *122*, 207–220. [CrossRef] [PubMed]
4. Camino, C.; Zarco-Tejada, P.J.; Gonzalez-Dug, V. Effects of Heterogeneity within tree crowns on airborne-quantified SIF and the CWSI as indicators of water stress in the context of precision agriculture. *Remote Sens.* **2018**, *10*, 604. [CrossRef]
5. Jia, M.; Zhu, J.; Ma, C.; Alonso, L.; Li, D.; Cheng, T.; Tian, Y.; Zhu, Y.; Yao, X.; Cao, W. Difference and potential of the upward and downward sun-induced chlorophyll fluorescence on detecting leaf nitrogen concentration in wheat. *Remote Sens.* **2018**, *10*, 1315. [CrossRef]
6. Kalaji, H.M.; Bąba, M.; Gediga, K.; Goltsev, V.; Samborska, I.A.; Cetner, M.D.; Dimitrova, S.; Piszcz, U.; Bielecki, K.; Karmowska, K.; et al. Chlorophyll fluorescence as a tool for nutrient status identification in rapeseed plants. *Photosynth. Res.* **2018**, *136*, 329–343. [CrossRef]
7. Thoren, D.; Schmidhalter, W. Nitrogen status and biomass determination of oilseed rape by laser-induced chlorophyll fluorescence. *Eur. J. Agron.* **2009**, *30*, 238–242. [CrossRef]
8. Tagliabue, G.; Panigada, C.; Dechant, B.; Baret, F.; Cogliati, S.; Colombo, R.; Migliavacca, M.; Rademske, P.; Schickling, A.; Schüttemeyer, D.; et al. Exploring the spatial relationship between airborne-derived red and far-red sun-induced fluorescence and process-based GPP estimates in a forest ecosystem. *Remote Sens. Environ.* **2019**, *231*, 1–19. [CrossRef]
9. Mohammed, G.H.; Colombo, R.; Middleton, E.M.; Rascher, U.; vanderTol, C.; Nedbal, L.; Goulas, Y.; Pérez-Priego, O.; Damm, A.; Meroni, M.; et al. Remote sensing of solar-induced chlorophyll fluorescence (SIF) in vegetation: 50 years of progress. *Remote Sens. Environ.* **2019**, *231*, 1–39. [CrossRef]
10. Muller, O.; Keller, B.; Zimmerman, L.; Jedmowski, C.; Kleits, E.; Pingle, V.; Acebron, K.; dos Santos, N.Z.; Steier, A.; Freiwald, L.; et al. Field phenotyping and an example of proximal sensing of photosynthesis under elevated CO_2. *IEEE IGARSS* **2018**, 8252–8254. [CrossRef]
11. Matese, A.; Toscano, P.; Di Gennaro, S.F.; Genesio, L.; Vaccari, F.P.; Primicerio, J.; Belli, C.; Zaldei, A.; Bianconi, R.; Gioli, B. Intercomparison of UAV, aircraft and satellite remote sensing platforms for precision viticulture. *Remote Sens.* **2015**, *7*, 2971–2990. [CrossRef]
12. Liu, L.; Zhang, Y.; Wang, J.; Zhao, C. Detecting solar-induced chlorophyll fluorescence from field radiance spectra based on the fraunhofer line principle. *IEEE Trans. Geosci. Remote Sens.* **2005**, *43*, 827–832. [CrossRef]
13. Porcar-Castell, A.; Tyystjärvi, E.; Atherton, J.; van der Tol, C.; Flexas, J.; Pfündel, E.E.; Moreno, J.; Frankenberg, C.; Berry, J.A. Linking chlorophyll a fluorescence to photosynthesis for remote sensing applications: Mechanisms and challenges. *J. Exp. Bot.* **2014**, *65*, 4065–4095. [CrossRef] [PubMed]
14. Thesien, A.F. Detecting chlorophyll fluorescence from orbit: The fraunhofer line depth model. In *From Laboratory Spectroscopy to Remotely Sensed Spectra of Terrestrial Ecosystems*, 1st ed.; Muttiah, R.S., Ed.; Springer: Dordrecht, The Netherlands, 2002; pp. 203–232. [CrossRef]
15. Cogliati, S.; Verhoef, W.; Kraft, S.; Sabater, N.; Alonso, L.; Vicent, J.; Moreno, J.; Drusch, M.; Colombo, R. Retrieval of sun-induced fluorescence using advanced spectral fitting methods. *Remote Sens. Environ.* **2015**, *169*, 344–357. [CrossRef]
16. Guanter, L.; Frankenberg, C.; Dudhia, A.; Lewis, P.E.; Gómez-Dans, J.; Kuze, A.; Suto, H.; Grainger, R.G. Retrieval and global assessment of terrestrial chlorophyll fluorescence from GOSAT space measurements. *Remote Sens. Environ.* **2012**, *121*, 236–251. [CrossRef]
17. Sun, Y.; Frankenberg, C.; Jung, M.; Joiner, J.; Guanter, L.; Köhler, P.; Magney, T. Overview of Solar-Induced chlorophyll Fluorescence (SIF) from the Orbiting Carbon Observatory-2: Retrieval, cross-mission comparison, and global monitoring for GPP. *Remote Sens. Environ.* **2018**, *209*, 808–823. [CrossRef]
18. Zhang, Y.; Xiao, X.; Zhang, Y.; Wolf, S.; Zhou, S.; Joiner, J.; Guanter, L.; Verma, M.; Sun, Y.; Yang, I.; et al. On the relationship between sub-daily instantaneous and daily total gross primary production: Implications for interpreting satellite-based SIF retrievals. *Remote Sens. Environ.* **2018**, *205*, 276–289. [CrossRef]
19. Ni, Z.; Lu, Q.; Huo, H.; Zhang, H. Estimation of chlorophyll fluorescence at different scales: A review. *Sensors* **2019**, *19*, 3000. [CrossRef]

20. Siegmann, B.; Alonso, L.; Celesti, M.; Cogliati, S.; Colombo, R.; Damm, A.; Douglas, S.; Guanter, L.; Hanuš, J.; Kataja, K.; et al. The high-performance airborne imaging spectrometer HyPlant—From raw images to top-of-canopy reflectance and fluorescence products: Introduction of an automatized processing chain. *Remote Sens.* **2019**, *11*, 2760. [CrossRef]
21. Cogliati, S.; Colombo, R.; Celesti, M.; Tagliabue, G.; Rascher, U.; Schickling, A.; Rademske, P.; Alonso, L.; Sabater, N.; Schuettemeyer, D.; et al. Red and far-red fluorescence emission retrieval from airborne high resolution spectra collected by the hyplant-fluo sensor. *IEEE IGARSS* **2018**, 3935–3938. [CrossRef]
22. Bandopadhyay, S.; Rastogi, A.; Juszczak, R.; Rademske, P.; Schickling, A.; Cogliati, S.; Julitta, T.; Mac Arthur, A.; Hueni, A.; Tomelleri, E.; et al. Examination of Sun-induced Fluorescence (SIF) signal on heterogeneous ecosystem platforms using 'HyPlant'. In Proceedings of the European Geosciences Union General Assembly (EGU), Vienna, Austria, 8–13 April 2018.
23. Tagliabue, G.; Panigada, C.; Dechant, B.; Baret, F.; Cogliati, S.; Colombo, R.; Migliavacca, M.; Rademske, P.; Schickling, A.; Schuettemeyer, D.; et al. Sun-Induced Fluorescence and photosynthesis estimation in a mixed forest ecosystem using high resolution airborne imagery. In Proceedings of the American Geophysical Union, Fall Meeting, Washington, DC, USA, 12–14 December 2018.
24. European Space Agency (ESA). Available online: https://earth.esa.int/web/guest/missions/esa-future-missions/flex (accessed on 9 April 2020).
25. Rascher, U.; Alonso, L.; Burkart, A.; Cilia, C.; Cogliati, S.; Colombo, R.; Damm, A.; Drusch, M.; Guanter, L.; Hanus, J.; et al. Sun-induced fluorescence—A new probe of photosynthesis: First maps from the imaging spectrometer HyPlant. *Glob. Change Biol.* **2015**, *21*, 4673–4684. [CrossRef] [PubMed]
26. Wieneke, S.; Ahrends, H.; Damm, A.; Pinto, F.; Stadler, A.; Rossini, M.; Rascher, U. Airborne based spectroscopy of red and far-red sun-induced chlorophyll fluorescence: Implications for improved estimates of gross primary productivity. *Remote Sens. Environ.* **2016**, *184*, 654–667. [CrossRef]
27. Ni, Z.; Liu, Z.; Li, Z.L.; Nerry, F.; Huo, H.; Sun, R.; Yang, P.; Zhang, W. Investigation of atmospheric effects on retrieval of Sun-Induced Fluorescence using hyperspectral imager. *Sensors* **2016**, *16*, 480. [CrossRef] [PubMed]
28. Bendig, J.; Gautam, D.; Malenovský, Z.; Lucieer, A. Influence of cosine corrector and uas platform dynamics on airborne spectral irradiance measurements. *IEEE IGARSS* **2018**, 8822–8825. [CrossRef]
29. Bandopadhyay, S.; Rastogi, A.; Juszczak, R. Review of Top-of-Canopy Sun-Induced Fluorescence (SIF) studies from ground, UAV, airborne to spaceborne observations. *Sensors* **2020**, *20*, 1144. [CrossRef]
30. Zarco-Tejada, J.P.; Catalina, A.; González, M.R.; Martín, P. Relationships between net photosynthesis and steady-state chlorophyll fluorescence retrieved from airborne hyperspectral imagery. *Remote Sens. Environ.* **2013**, *136*, 247–258. [CrossRef]
31. Atherton, J.; Mac Arthur, A.; Hakala, T.; Maseyk, K.; Robinson, I.; Liu, W.; Honkavaara, E.; Porcar-Castell, A. Drone measurements of solar-induced chlorophyll fluorescence acquired with a low-weight DFOV spectrometer system. *IEEE IGARSS* **2018**, 8834–8836. [CrossRef]
32. Milton, E.J.; Schaepman, M.E.; Anderson, K.; Kneubühler, M.; Fox, N. Progress in field spectroscopy. *Remote Sens. Environ.* **2009**, *113*, 92–109. [CrossRef]
33. Mac Arthur, A.; Robinson, I. A critique of field spectroscopy and the challenges and opportunities it presents for remote sensing for agriculture, ecosystems, and hydrology. In Proceedings of the SPIE 9637 Remote Sensing for Agriculture, Ecosystems, and Hydrology XVII, Toulouse, France, 14 October 2015. [CrossRef]
34. Mac Arthur, A.; Robinson, I.; Rossini, M.; Davis, N.; MacDonald, K. A dual-field-of-view spectrometer system for reflectance and fluorescence measurements (Piccolo Doppio) and correction of etaloning. In Proceedings of the 5th International Workshop on Remote Sensing of Vegetation Fluorescence, Paris, France, 22–24 April 2014; Available online: https://www.research.ed.ac.uk/portal/files/17385047/A_DFOV_spectrometer_system_for_reflectance_and_fluorescence_Piccolo.pdf (accessed on 9 April 2020).
35. Mac Arthur, A.; Robinson, I.; Hagdorn, M.; Wood, J.; Kershaw, R.; Taylor, R. Piccolo spectrometer system for reflectance and fluorescence measurement from mobile and fixed platforms. In Proceedings of the Innovative Optical Tools for Proximal Sensing of Ecophysiological Processes (OPTIMISE), Vienna, Austria, 23–28 April 2017.
36. Bendig, J.; Malenovský, Z.; Gautam, D.; Lucieer, A. Solar-induced chlorophyll fluorescence measured from an unmanned aircraft system—Sensor etaloning and platform motion correction. *IEEE Trans. Geosci. Remote Sens.* **2019**. [CrossRef]

37. JB Hyperspectral Devices. Available online: https://www.jb-hyperspectral.com/ (accessed on 7 July 2019).
38. Burkart, A.; Cogliati, S.; Schickling, A.; Rascher, U. A novel UAV-based ultra-light weight spectrometer for field spectroscopy. *IEEE Sens. J.* **2014**, *14*, 62–67. [CrossRef]
39. Becerra, J.; Martin, M.P.; Pacheco-Labrador, J.; Gonzalez-Cascon, R.; Melendo-Vega, J.R.; Angás, J. Chlorophyll Estimation in Mediterranean Quercus *ilex* tree canopies with hyperspectral vegetation indices at leaf and crown scales. In Proceedings of the IEEE YP Remote Sensing Conference, Aachen, Germany, 7–8 June 2018.
40. Garzonio, R.; Di Mauro, B.; Colombo, R.; Cogliati, S. Surface reflectance and sun-induced fluorescence spectroscopy measurements using a small hyperspectral UAS. *Remote Sens.* **2017**, *9*, 472. [CrossRef]
41. Cogliati, S.; Rossini, M.; Meroni, M.; Barducci, A.; Julitta, T.; Colombo, R. Unattended instruments for ground-based hyperspectral measurements: Development and application for plant photosynthesis monitoring. In Proceedings of the American Geophysical Union, Fall Meeting, San Francisco CA, USA, 5–9 December 2011.
42. Anderson, K.; Rossini, M.; Pacheco-Labrador, J.; Balzarolo, M.; Mac Arthur, A.; Fava, F.; Julitta, T.; Vescovo, L. Inter-comparison of hemispherical conical reflectance factors (HCRF) measured with four fibre-based spectrometers. *Opt. Express* **2013**, *21*, 605–617. [CrossRef] [PubMed]
43. Mathworks. Field Spectroscopy Facility Post Processing Toolbox—File Exchange—MATLAB Central. Available online: https://uk.mathworks.com/matlabcentral/fileexchange/31547-field-spectroscopy-facility-post-processing-toolbox (accessed on 9 April 2020).
44. Maseyk, K.; Atherton, J.; Thomas, R.; Wood, K.; Tausz-Posch, S.; Mac Arthur, A.; Porcar-Castell, A.; Tausz, M. Investigating forest photosynthetic response to elevated CO_2 using UAV-based measurements of Solar Induced Fluorescence. *IEEE IGARSS* **2018**, 8830–8833. [CrossRef]
45. Hart, K.M.; Curioni, G.; Blaen, P.; Harper, N.J.; Miles, P.; Lewin, K.F.; Nagy, J.; Bannister, E.J.; Cai, X.M.; Thomas, R.M.; et al. Characteristics of free air carbon dioxide enrichment of a northern temperate mature forest. *Glob. Change Biol.* **2019**, *26*, 1023–1037. [CrossRef] [PubMed]
46. Mihai, L.; Mac Arthur, A.; Hueni, A.; Robinson, I.; Sporea, D. Optimized spectrometers characterization procedure for near ground Support of ESA FLEX Observations: Part 1 Spectral Calibration and Characterization. *Remote Sens.* **2018**, *10*, 289. [CrossRef]
47. Herrmann, I.; Vosberg, S.K.; Townsend, P.A.; Conley, S.P. Spectral data collection by dual Field-of-View System under Changing Atmospheric Conditions—A case study of estimating early season soybean populations. *Sensors* **2019**, *19*, 457. [CrossRef]
48. Bendig, J.; Malenovský, Z.; Siegmann, B.; Rademske, P.; Krause, A.; Gruenhagen, L.; Koeing, S.; Prum, M.; Gautam, D.; Rascher, U.; et al. UAS-based chlorophyll fluorescence measurements of barley canopies—Results from FLEXsense 2019. In Proceedings of the International Network on Remote Sensing of Terrestrial and Aquatic Fluorescence, Davos, Switzerland, 5–8 March 2019.
49. Gautam, D.; Lucieer, A.; Bendig, J.; Malenovský, Z. Footprint determination of a spectroradiometer mounted on an unmanned aircraft system. *IEEE Trans. Geosci. Remote Sens.* **2019**. [CrossRef]
50. Gautam, D.; Lucieer, A.; Malenovskz, Z.; Watson, C. Comparison of MEMS-Based and FOG-Based IMUs TO Determine Sensor Pose on an Unmanned Aircraft System. *J. Surv. Eng.* **2017**, *143*. [CrossRef]
51. Gautam, D.; Watson, C.; Lucieer, A.; Malenovský, Z. Error Budget for Geolocation of Spectroradiometer Point Observations from an Unmanned Aircraft System. *Sensors* **2018**, *18*, 3465. [CrossRef]
52. Gautam, D.; Lucieer, A.; Watson, C.; McCoull. Lever-arm and boresight correction, and field of view determination of a spectroradiometer mounted on an unmanned aircraft system. *ISPRS J. Photogramm. Remote Sens.* **2019**, *155*, 25–36. [CrossRef]
53. Julitta, T.; Burkart, A.; Colombo, R.; Rossini, M.; Schickling, A.; Migliavacca, M.; Cogliati, S.; Wutzler, T.; Rascher, U. Accurate measurements of fluorescence in the O2A and O2B band using the FloX spectroscopy system—Results and prospects. In Proceedings of the Potsdam GHG Flux Workshop: From Photosystems to Ecosystems, Potsdam, Germany, 24–26 October 2017.
54. Cogliati, S.; Celesti, M.; Cesana, I.; Miglietta, F.; Genesio, L.; Julitta, T.; Schuettemeyer, D.; Drusch, M.; Rascher, U.; Jurado, P.; et al. A spectral fitting algorithm to retrieve the fluorescence spectrum from canopy radiance. *Remote Sens.* **2019**, *11*, 1840. [CrossRef]
55. Drusch, M.; Moreno, J.; Del Bello, U.; Franco, R.; Goulas, Y.; Huth, A.; Kraft, S.; Middleton, E.; Miglietta, F.; Mohammed, G.; et al. The FLuorescence EXplorer mission concept—ESA's Earth Explorer 8. *IEEE Trans. Geosci. Remote Sens.* **2018**, *55*, 1273–1284. [CrossRef]

56. Damm, A.; Guanter, L.; Laurent, C.E.; Schaepman, M.E.; Schickling, A.; Rascher, U. FLD-based retrieval of sun-induced chlorophyll fluorescence from medium spectral resolution airborne spectroscopy data. *Remote Sens. Environ.* **2014**, 256–266. [CrossRef]
57. Sabater, N.; Vicent, J.; Alonso, L.; Verrelst, J.; Middleton, E.M.; Porcar-Castell, A.; Moreno, J. Compensation of Oxygen transmittance effects for proximal sensing retrieval of canopy–leaving sun–induced chlorophyll fluorescence. *Remote Sens.* **2018**, *10*, 1551. [CrossRef]
58. Wang, N.; Bartholomeus, H.; Kooistra, L.; Suomalainen, J.; Brede, B.; Novani, M.; Masiliunas, D.; Clevers, J. Measuring temporal patterns of crop sun-induced chlorophyll fluorescence at canopy and plot scale. In Proceedings of the 11th EARSeL SIG IS Workshop, Brno, Czech Republic, 6–8 February 2019.
59. Damm, A.; Erler, A.; Hillen, W.; Meroni, M.; Schaepman, M.E.; Verhoef, W.; Rascher, U. Modeling the impact of spectral sensor configurations on the FLD retrieval accuracy of sun-induced chlorophyll fluorescence. *Remote Sens. Environ.* **2011**, *115*, 1882–1892. [CrossRef]
60. Alonso, L.; Sabater, N.; Vicent, J.; Mihai, N.; Moreno, J. Atmospheric and instrumental effects on the fluorescence remote sensing retrieval. *IEEE IGARSS* **2018**. [CrossRef]
61. Li, D.; Zheng, H.; Xu, X.; Lu, N.; Yao, X.; Jiang, J.; Wang, X.; Tian, Z.; Zhu, Z.; Cao, W.; et al. BRDF effect on the estimation of canopy chlorophyll content in paddy rice from UAV-based hyperspectral imagery. *IEEE IGARSS* **2018**, 6464–6467. [CrossRef]
62. Burkart, A.; Aasen, H.; Alonso, L.; Menz, G.; Bareth, G.; Rascher, U. Angular dependency of hyperspectral measurements over wheat characterized by a novel UAV based goniometer. *Remote Sens.* **2015**, *7*, 725–746. [CrossRef]
63. Pinto, F.; Müller-Linow, M.; Schickling, A.; Cendrero-Mateo, M.P.; Ballvora, A.; Rascher, U. Multiangular observation of canopy sun-induced chlorophyll fluorescence by combining imaging spectroscopy and stereoscopy. *Remote Sens.* **2017**, *9*, 415. [CrossRef]